Journal of Controlled Release 383 (2025) 113764

Contents lists available at ScienceDirect

Journal of Controlled Release

journal homepage: www.elsevier.com/locate/jconrel

Polymersome-enabled brain codelivery of STAT3 siRNA and CpG oligonucleotide boosts chemo-immunotherapy of malignant glioma☆

Songsong Zhao [a], Zhiwei Sun [a], Mingyu Xia [a], Beibei Guo [a], Yanyi Qu [a], Jingyi Wang [a], Zhiyuan Zhong [a,b,*], Fenghua Meng [a,*]

[a] Biomedical Polymers Laboratory, College of Chemistry, Chemical Engineering and Materials Science, and State Key Laboratory of Radiation Medicine and Protection, Soochow University, Suzhou 215123, PR China
[b] College of Pharmaceutical Sciences, Soochow University, Suzhou 215123, PR China

ARTICLE INFO

Keywords:
Malignant glioma
Cancer immunotherapy
Tumor immune microenvironment
Targeted delivery
STAT3
Temozolomide

ABSTRACT

Malignant glioma represents one of the most aggressive primary tumors of the central nervous system. The immunotherapy of glioma is restrained by low immunogenicity, an immunosuppressive environment, and challenges in delivering therapeutics and immune-modulating agents. Here, we demonstrate that the systemic brain codelivery of STAT3 siRNA and CpG oligonucleotide using ApoE peptide-functionalized nano-polymersomes (tNano-S&C) significantly boosts the efficacy of chemo-immunotherapy for malignant glioma when combined with temozolomide (TMZ). The administration of STAT3 siRNA via tNano-S&C effectively knocked down STAT3 expression in glioma cells, resulting in increased sensitivity to TMZ treatment and enhancing immunogenic cell death. Furthermore, tNano-S&C was efficiently taken up by dendritic cells (DCs), inducing DC maturation and proinflammatory cytokine secretion. Interestingly, intravenous injections of tNano-S&C in orthotopic murine glioma LCPN models revealed elevated accumulation at the tumor site, in cervical lymph nodes (CLNs) and the spleen, and within antigen-presenting cells (APCs). This delivery system effectively enhanced the outcomes of chemo-immunotherapy with TMZ, leading to a marked extension of median survival time and complete regression in 25% mice. tNano-S&C treatment reduced M2 phenotype glioma associated macrophages and regulatory T cells, while increasing the recruitment of cytotoxic T lymphocytes. These findings suggest that this polymersome-enabled brain codelivery of STAT3 siRNA and immunoadjuvants provides an appealing strategy to effectively reshape the tumor immune microenvironment and boost the efficacy of chemo-immunotherapy of malignant glioma.

1. Introduction

Malignant glioma is an aggressive malignancy of the central nervous system with a dismal prognosis, characterized by a five-year survival rate of less than 10%. Despite rigorous clinical interventions, including gross total resection, high-dose radiation therapy (RT), temozolomide (TMZ) chemotherapy and combined therapy like tumor treating fields (TTFields) and antibody therapies [1,2], high rates of tumor recurrence are recorded, often within months of standard treatment. Notably, over 50% of malignant glioma patients develop resistance to TMZ, resulting in poor outcomes without efficient subsequent treatment options and a recurrence rate exceeding 90% [3,4].

In the past decade, extensive efforts have been dedicated to mitigating TMZ resistance and reducing tumor recurrence. Strategies aimed at enhancing glioma cell sensitivity to TMZ have focused on down-regulating pathways involved in DNA repair and stem cell formation in tandem with TMZ treatment [4–8]. Notably, immunotherapy has transformed the treatment landscape for melanoma, lung cancer and liver cancers, and shows great potential in minimizing tumor relapse by stimulating immune system against tumor cells through using immune adjuvants [9,10], cytokines [11] or T-cell chemokines [12–14]. However, combination therapies for malignant glioma have yielded suboptimal results. The clinical trials involving immunotherapies, such as tumor vaccines, Chimeric Antigen Receptor T-Cell immunotherapy

☆ This article is part of a Special issue entitled: 'SI Feijen' published in Journal of Controlled Release.

* Corresponding authors at: Biomedical Polymers Laboratory, College of Chemistry, Chemical Engineering and Materials Science, and State Key Laboratory of Radiation Medicine and Protection, Soochow University, Suzhou 215123, PR China.
E-mail addresses: zyzhong@suda.edu.cn (Z. Zhong), fhmeng@suda.edu.cn (F. Meng).

https://doi.org/10.1016/j.jconrel.2025.113764
Received 23 November 2024; Received in revised form 22 March 2025; Accepted 21 April 2025
Available online 22 April 2025

(CAR-T) therapy, and immune checkpoint blockade therapy (ICB) targeting programmed death protein-1 (PD-1), have not outperformed the standard treatments. Trials involving TLR9 agonist (such as CpG oligodeoxynucleotide) [15], PD-1 monoclonal antibody in combination with radiotherapy and TMZ [16], and peptide vaccines targeting epithelial growth factor receptor variants III (EGFRvIII) combined with TMZ [17] have all resulted in unsatisfactory outcomes. These disappointing results are largely attributed to the low immunogenicity of malignant glioma, its immunosuppressive microenvironment (characterized by low T-cell infiltration and abundant immunosuppressive cells/factors), and the inaccessibility of therapeutics and immune-modulating agents across the blood-brain barrier (BBB) [18,19].

In this study, we report the development of ApoE peptide-functionalized nano-polymersomes for the brain codelivery of STAT3 siRNA (siSTAT3) and CpG oligodeoxynucleotide (CpG ODN) (tNano-S&C) as a strategy to reverse the immunosuppressive tumor microenvironment (TME) and enhance the efficacy of chemo-immunotherapy of malignant glioma (Scheme 1). The overexpression of STAT3 in both glioma cells and antigen-presenting cells (APCs) has been identified as a key factor contributing to tumor malignancy, drug resistance and the suppressive TME [20–22]. Silencing of STAT3 is expected to promote immunogenic cell death (ICD) of tumor cells by translocation of calreticulin (CRT) to the cell surface and a significant reduction in the expression of "don't eat me" signal [23,24]. We have previously reported that ApoE-functionalized polymersomes can deliver CpG to glioma via intranasal or systemic injection, thereby elevating DC maturation and immune responses in murine glioma models [25,26]. Combination therapies utilizing STAT3 inhibition and CpG, especially CpG-STAT3 conjugates and nanoformulations (like AIRISE-02), have shown anti-tumor efficacy in hematologic malignancies and some solid tumors when administered locally [27–29], but their therapeutic effect in glioma remains limited [30]. This study represents the first report of the brain co-delivery of siSTAT3 and CpG for malignant glioma, providing a novel and unique approach to boost chemo-immunotherapy. Interestingly, tNano-S&C markedly increased the anti-tumor activity of TMZ and stimulated immune responses in glioma-bearing mice, resulting in greatly improved survival rates and even tumor eradication. This polymersome-enabled brain codelivery of siSTAT3 and immunoadjuvant provides a potential therapeutic strategy for malignant glioma.

2. Experimental section

2.1. Preparation and characterization of tNano-S&C

tNano-S&C was prepared by adding 100 μL DMF solution of ApoE-PEG-P(TMC-DTC) and PEG-P(TMC-DTC)-Spe at a molar ratio of 2/8 (polymer conc.: 40 mg mL^{-1}) into 900 μL phosphate buffer (PB, 2.0 mM, pH 6.0) containing 200 μg siSTAT3 and 100 μg CpG under stirring. After 5 min, the dispersion was dialyzed (MWCO: 1000 kDa) sequentially in PB (2 mM, pH 6.0) for 3 h, and PB (10 mM, pH 7.4) for 3 h. Non-targeting polymersomes coloaded with siSTAT3 and CpG (Nano-S&C) and ApoE-functionalized polymersomes loaded with only siSTAT3 (tNano-S) or CpG (tNano-C) were prepared in same way. Particle size, zeta potential, drug loading contents and loading stability as well as morphology of tNano-S&C were evaluated.

2.2. STAT3 silencing by tNano-S and tNano-S&C

LCPN cells were cultured in 24-well plates (2×10^5/well) overnight, and incubated with tNano-S, Nano-S, Lipo-S (siSTAT3 conc.: 1.33 μg mL^{-1}) or PBS ($n = 3$). Lipo-S was prepared using lipofectamine 3000 to complex siSTAT3 according to the supplier's protocol. After 48 h, total RNA was isolated and purified from cell lysate using RNA-easy Isolation Reagent. STAT3 mRNA expression was determined using quantitative real-time polymerase chain reaction (qRT-PCR) (GAPDH as internal reference), and data were analyzed using $2^{-\Delta\Delta CT}$ method. Murine GL261 cells (4×10^5/well) and human U87 MG cells (2×10^5/well) were treated with free S, Nano-S, Lipo-S, tNano-S or tNano-S&C (siSTAT3 conc.: 1.33 μg mL^{-1}, CpG conc.: 0.665 μg mL^{-1}) and measured similarly ($n = 3$).

To determine the silencing of STAT3 and downstream proteins using western blotting, LCPN cells seeded in 24-well plates (2×10^5/well) overnight were incubated with free siSTAT3, Nano-S, tNano-S, tNano-C or tNano-S&C (siSTAT3 conc.: 2.66 μg mL^{-1}, CpG conc.: 1.33 μg mL^{-1}) for 48 h ($n = 3$). The cells were then treated with RIPA, and proteins were isolated, purified and quantified. 40 μg protein samples were subject to electrophoresis using standard procedure. Primary antibodies targeting STAT3, pSTAT3, MGMT, and Bcl-2, and HRP-labeled secondary antibody were used. The band images were taken using chemiluminescence detector (GAPDH as internal reference).

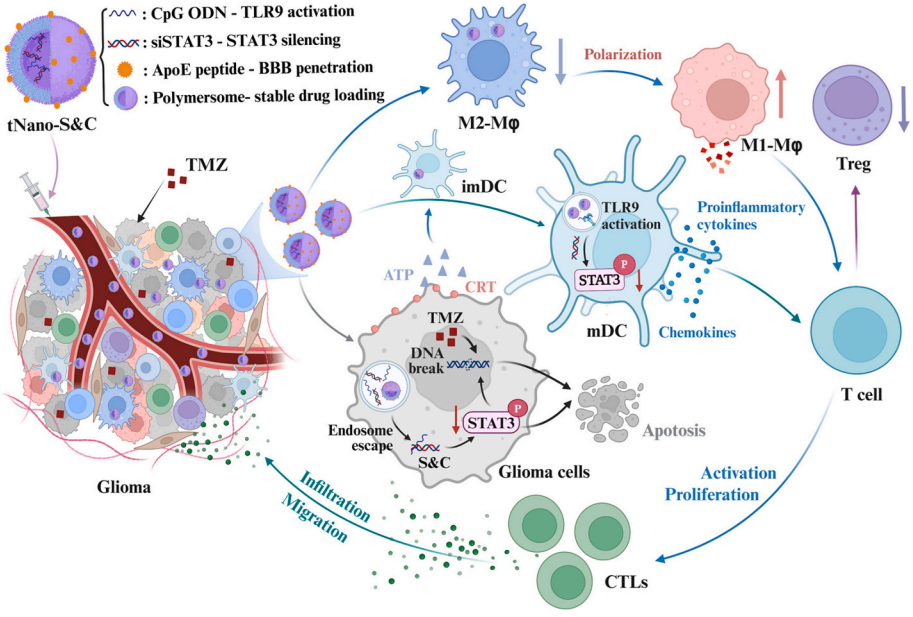

Scheme 1. Illustration of systemic brain codelivery of siSTAT3 and CpG ODN by ApoE peptide-functionalized polymersomes (tNano-S&C) for boosting the chemo-immunotherapy of malignant glioma with TMZ.

2.3. Cytotoxicity and ICD of LCPN cells

LCPN cells were seeded in 96-well plates (1×10^3/well, 80 μL) overnight. TMZ, TMZ+tNano-S, or TMZ+tNano-S&C were added (TMZ conc.: 0.01–100 μg mL^{-1}; siSTAT3 conc.: 1.33 μg mL^{-1}, CpG conc.: 0.665 μg mL^{-1}) were added. After incubation for 48 h, cells were subject to standard MTT assays, and the absorbance at 570 nm was measured by microplate to calculate cell viability ($n = 3$). The cytotoxicity of tNano-S or tNano-S&C alone was studied by similar methods described above. tNano-S and tNano-S&C were added into LCPN cells for 48 h, then the viability was detected by MTT assay, respectively. The half maximal inhibitory concentrations (IC_{50}) of TMZ and S&C were calculated using prism software. MTT assays of GL261 cells (5×10^3/well) treated with TMZ, TMZ+tNano-S, and tNano-S&C (siSTAT3: 0.266 μg mL^{-1}, CpG: 0.133 μg mL^{-1}), or tNano-S and tNano-S&C (siSTAT3/CpG = 2/1) were similarly performed ($n = 6$).

For ICD detection, LCPN cells were cultured in 24-well plates (1×10^5/well) overnight, and incubated with PBS, tNano-S, tNano-S&C, TMZ, TMZ+tNano-S and TMZ+tNano-S&C (siSTAT3 conc.: 1.33 μg mL^{-1}, CpG conc.: 0.665 μg mL^{-1}, TMZ conc.: 10 μg mL^{-1}, $n = 3$). After 24 h, culture medium was collected for quantifying ATP by enhanced ATP assay kits, and cells were sequentially incubated with anti-CD16/32 (20 min), CRT antibody (30 min) and Alexa fluor® 647-conjugated secondary antibody (30 min, 4 °C) before FC measurements.

2.4. Stimulation of APCs

BMDCs, BMDM and BV2 cells were separately cultured in 12-well plates (1×10^6/well) overnight, and treated with tNano-S&C, Nano-S&C, free S&C, tNano-S, tNano-C, or a mixture of tNano-S and tNano-C (tNano-S+C) (siSTAT3 conc.: 1.0 μg mL^{-1}; CpG conc.: 0.5 μg mL^{-1}, $n = 3$). PBS, IL-4 (20 ng mL^{-1}) and LPS (100 ng mL^{-1}) plus IFN-γ (10 ng mL^{-1}) were used as controls. After incubating for 24 h, BMDCs were stained with FITC-anti-CD11c, PE-anti-CD86 and APC-anti-CD80 antibodies, and BMDM and BV2 cells were stained with FITC-anti-CD11b, PE-anti-F4/80 and Alexa fluor® 647-anti-CD206 antibodies before FC measurements.

To study the effect of ICD of LCPN cells on stimulating APCs, LCPN cells seeded in 12-well plates (1×10^5/well) overnight were first treated with tNano-S, tNano-C, tNano-S&C, TMZ+tNano-S&C, Nano-S&C, or free S&C (siSTAT3 conc.: 1 μg mL^{-1}, CpG conc.: 0.5 μg mL^{-1}, TMZ conc.: 10 μg mL^{-1}, $n = 3$) for 12 h. Then BMDCs, BMDM or BV2 cells (1×10^6/well) were added and incubated for 24 h. All cells were collected, and stained with percp/cy5.5-anti-CD45 for distinguishing immune cells from LCPN cells. The following antibody staining and FC measurements were the same as above.

To determine the effect of ICD of LCPN cells on the RNA silencing in BMDCs, LCPN cells (1×10^5/well) and BMDCs (1×10^6/well) were respectively cultured in the upper and lower chamber of 24-well transwell units in RPMI 1640 medium containing 10% FBS, 1% penicillin-ptreptomycin, EGF and FGF at 5% CO_2 and 37 °C. Then tNano-S, tNano-C, Nano-S&C, tNano-S&C, or TMZ+tNano-S&C were added into the upper chamber (siSTAT3 conc.: 1 μg mL^{-1}, CpG conc.: 0.5 μg mL^{-1}, TMZ conc.: 10 μg mL^{-1}) and cultured for 24 h. Culture medium was taken for the determination of concentrations of IFN-β using ELISA kit ($n = 3$). BMDCs were collected, and RNA was extracted using RNA-easy Isolation Reagent. The expression of STAT3 mRNA and CXCL10 mRNA were determined with qRT-PCR and analyzed using $2^{-\Delta\Delta CT}$ method ($n = 3$).

2.5. Biodistribution of tNano-S&C in orthotopic LCPN tumor-bearing mice

All animal experiments were approved by the Animal Care and Use Committee of Soochow University (P. R. China) and all protocols for the animal studies conformed to the Guide for the Care and Use of Laboratory Animals (approval numbers: 202109A0046, 202207A0585, 202211A0248).

Biodistribution of tNano-S&C was studied with cy7-labeled CpG as a probe in orthotopic LCPN models that was established as previously described [26]. Briefly, 5×10^4 LCPN cells in 5 μL cold PBS containing 25 vol.% matrigel was injected into left striatum of C57BL/6 mice (Injection coordinates: 1.9 mm lateral, 0.5 mm anterior and 3.1 mm deep) and the syringe retained in place for 5 min. This day was designated as day 0. On day 7, 200 μL tNano-S&C, Nano-S&C and free S&C (siSTAT3: 2 mg kg^{-1}, CpG: 1 mg kg^{-1}, cy7: 0.3 μg per mouse) were intravenously (i.v.) injected via tail veins ($n = 3$). At 4, 8 and 12 h post-injection, in vivo imaging of the mouse heads was performed, and at 12 h, ex vivo fluorescence images of heart, liver, spleen, lung, kidney, cancerous brain and cervical lymph nodes (CLNs) were taken by a NIR imaging system and semi-quantified using Living Image software. The orthotopic glioma and remaining normal brain tissue, all CLNs at both sides of the neck, and the spleen were then collected, ground and centrifuged to obtain single-cell suspensions, and respectively tagged by flow cytometric antibodies for macrophages ($CD45^+CD11b^+F4/80^+$), DCs ($CD45^+CD11c^+$) and B cells ($CD45^+B220^+$). Mean fluorescence intensity (MFI) of cy7 and cell counts within different tissues and APCs were measured using FC and organs of mice injected with PBS were used as controls.

2.6. Anti-glioma efficacy of TMZ+tNano-S&C in orthotopic GBM mice

On day 3 post-inoculation, LCPN mice were randomly divided into eight groups ($n = 6$): PBS, free S&C, Nano-S&C, tNano-S, tNano-C, tNano-S+C, tNano-S&C, and TMZ+tNano-S&C. On days 3, 5, 7, 17 and 19, 200 μL nanoformulations were i.v. administered via tail veins (siSTAT3: 2 mg kg^{-1} and CpG: 1 mg kg^{-1}). For TMZ and combination groups, TMZ was administered orally continuously on days 3–7 (40 mg kg^{-1}). Body weight and survival of the mice were monitored. On day 23, one mouse from groups (PBS, Nano-S&C, tNano-S&C and TMZ+tNano-S&C) was randomly selected to collect the brain (containing tumor) and major organs for hematoxylin and eosin (H&E) analysis.

In a separate experiment, on day 3 post-inoculation, LCPN mice were randomly assigned to five groups ($n = 4$): PBS, TMZ, TMZ+tNano-S, TMZ+tNano-C, and TMZ+tNano-S&C. The dosing regimen, treatment schedule and monitoring of the mice were the same as above, except that 120 μL blood was collected on day 7 for the quantification of cytokines (TNF-α, IFN-γ and IL-10) using ELISA kits.

Orthotopic GL261 mice were built using the same method as LCPN model and treated with five i.v. injections of tNano-S&C (siSTAT3: 2 mg kg^{-1} and CpG: 1 mg kg^{-1}) on days 3, 5, 7, 17 and 19 post-inoculation ($n = 5$). Body weight and survival curves were monitored.

2.7. Immunostimulatory efficacy of TMZ+tNano-S&C in orthotopic LCPN mice

On day 9 post-inoculation, LCPN mice were randomly divided into six groups ($n = 6$): PBS, tNano-S, tNano-C, tNano-S&C, TMZ+tNano-S&C, and TMZ+Nano-S&C. On days 9, 11 and 13, 200 μL nanoformulations were i.v. administered (siSTAT3: 2 mg kg^{-1} and CpG: 1 mg kg^{-1}), and for combination group, TMZ was orally continuously on days 9–13 (40 mg kg^{-1}). On day 14, one mouse from each group was randomly selected to prepare glioma-bearing brain slices for immunofluorescence assays. The slices were stained with CRT antibody (ICD), CD80 antibody (DCs), CD8 antibody ($CD8^+$T cells), Iba1 antibody (Mϕ, macrophage) and iNOS antibody (M1M), or PD-L1 antibody (immune checkpoint). This was followed by treating with Alexa Fluor® 647 goat anti-rabbit IgG H&L secondary antibody (Alexa Fluor® 488 labelling for Iba1) and imaging with CLSM. The remaining five mice of each group were sacrificed and blood was collected for cytokine (TNF-α, IFN-γ and IL-10) quantification using ELISA kits ($n = 5$). The extracted tumors, CLNs and spleens were collected and lysed into single-cell suspensions

placed in cold PBS. Cells were stained with Zombie NIR™ Fixable Viability Kit (30 min) for labelling living cells, blocked with anti-CD16/32 (20 min), and stained with fluorescence-labeled antibodies (30 min) according to manufacturer's protocols. The cell samples were then measured using FC and analyzed using FlowJo software for the proportions of mDC ($CD45^+CD11c^+CD80^+CD86^+$), $CD8^+$T cells ($CD45^+CD3^+CD8^+$), M1M ($CD45^+CD11b^+F4/80^+CD206^-$) and regulatory T cells (Treg, $CD45^+CD3^+CD4^+foxp3^+$).

2.8. Statistical analysis

Data was presented as mean ± standard deviation. Significant differences among groups were determined using one-way ANOVA with Tukey's multiple comparison tests using GraphPad Prism 8.0. Kaplan-Meier survival rates were analyzed using the log-rank test for comparison. Statistical significance was defined as follows: * $p < 0.05$ means significant difference, ** $p < 0.01$, *** $p < 0.001$ and **** $p < 0.0001$ indicate highly significant difference.

3. Results and discussion

3.1. Construction and characterization of tNano-S&C

BBB-penetrating polymersomes co-loaded with siSTAT3 and CpG (denoted as tNano-S&C) were constructed through the co-self-assembly of poly(ethylene glycol)-b-poly(trimethylene carbonate-co-dithiolene trimethylene carbonate)-b-spermine (PEG-P(TMC-DTC)-Spe) and ApoE peptide-functionalized copolymer (ApoE-PEG-P(TMC-DTC), 20 mol%) in aqueous solutions containing siSTAT3 and CpG (Fig. 1a). Polymersomes loaded with only siSTAT3 or CpG were obtained using the same method and denoted as tNano-S and tNano-C, respectively. This approach achieved drug loading efficiencies (DLE) over 95% at theoretical drug loading contents (DLC) ≤ 20 wt.% (**Table S1, S2**). The efficient loading of siSTAT3 or CpG was attributed to their electrostatic interactions and hydrogen bonding with spermine within the polymersome interior. The empty polymersomes, tNano, demonstrated peaks of ApoE peptides in the ^{1}H NMR spectrum using D_2O as a solvent (**Fig. S1**), and exhibited the characteristic absorption peaks of ApoE peptide in the FT-IR spectrum (amino and guanidine: 3300–3500 cm^{-1} and 1550–1600 cm^{-1}, **Fig. S2**), confirming the presence of ApoE peptides on the surface and ensuring good targetability. Single drug-loaded polymersomes and dual-drug-loaded polymersomes all exhibited uniform sizes (44.0–50.2 nm) and neutral zeta potential (**Table S2**, Fig. 1b). TEM images of tNano-S&C showed spherical vesicles with an average size of ca. 45 nm (**Fig. S3a**). Notably, these formulations remained stable after over 30 days of storage, as well as upon 100-fold dilution, and incubation with PBS containing 10% serum (**Fig. S3b,c**). Agarose gel electrophoresis confirmed the stable encapsulation of siSTAT3 and CpG, and the reduction-responsive release of payload triggered by 10 mM glutathione (**Fig. S3d**).

3.2. Uptake and endosomal escape of tNano-S and tNano-S&C in LCPN cells

The cellular uptake and endosomal escape of siSTAT3-loaded polymersomes (tNano-S) in murine malignant glioma LCPN cells were evaluated using cy5-labeled siSTAT3 (cy5-siSTAT3) as a probe. CLSM images showed that tNano-S rapidly entered the cells, with marked escape of siRNA from endosomes observed over time (1, 2 to 4 h), as evidenced by a drastically decrease in the colocalization coefficient of

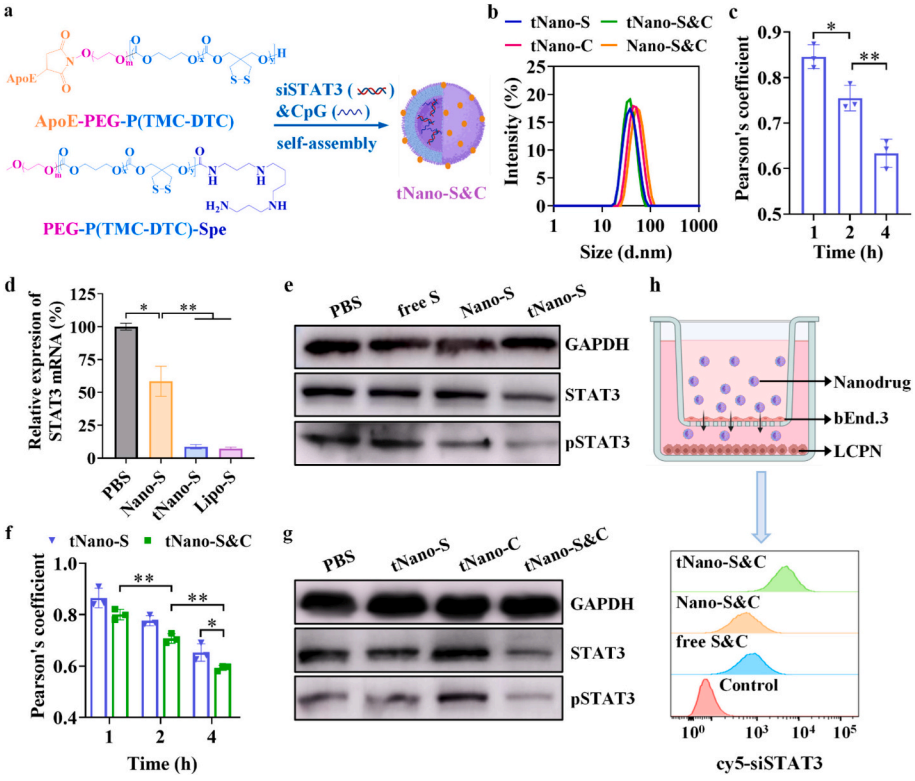

Fig. 1. In vitro characterization of tNano-S and tNano-S&C. a) Preparation and b) size distribution profiles of tNano-S and tNano-S&C. c) Pearson's coefficients to determine the co-localization of tNano-S with endosomes of LCPN cells derived from CLSM images (cy5-siSTAT3 as a probe, $n = 3$). d) qRT-PCR assay of STAT3 mRNA levels in LCPN cells treated with Nano-S and tNano-S for 48 h (siSTAT3 conc.: 1.33 μg mL^{-1}, n = 3). e) Expression of STAT3 and pSTAT3 in LCPN cells treated with tNano-S for 48 h (siSTAT3 conc.: 2.66 μg mL^{-1}, GAPDH as an internal reference). f) Pearson's coefficients of cy5-siSTAT3 and endosomes of LCPN cells treated with tNano-S and tNano-S&C (n = 3). g) Expression of STAT3 and pSTAT3 in LCPN cells treated with tNano-S and tNano-S&C for 48 h (siSTAT3 conc.: 2.66 μg mL^{-1}, CpG conc.: 1.33 μg mL^{-1}). h) Uptake of tNano-S&C by LCPN cells after penetrating BBB monolayer model. * $p < 0.05$, ** $p < 0.01$, and *** $p < 0.001$.

siSTAT3 and endosomes showing Pearson's coefficient of 0.85, 0.75 and 0.63, respectively (Fig. 1c). Given that STAT3 overexpression in glioma cells is a key factor contributing to tumor malignancy and drug resistance [20], we found that tNano-S significantly inhibited STAT3 mRNA expression in LCPN cells, achieving a silencing efficiency of 90%, similar as that of Lipo-S (92%) and 2.1-fold that of non-targeting control Nano-S (**, Fig. 1d). Western blot results further demonstrated the potency of tNano-S in down-regulating both total STAT3 and phosphorylated STAT3 (pSTAT3) levels compared to Nano-S and free siSTAT3 (Fig. 1e), reinforcing the active-targeted delivery to glioma cells. Remarkably, the dual-drug loaded polymersomes, tNano-S&C, also demonstrated 4.3-fold higher endocytosis than Nano-S&C and free S&C groups (**Fig. S4a**). Moreover, tNano-S&C group showed 1.2-fold greater cellular fluorescence, accelerated endosomal escape, and more pronounced inhibition of STAT3 and pSTAT3 expression compared to tNano-S group (**Fig. S4a,** Fig. 1f,g). This enhanced performance likely results from the binding of the released CpG to TLR9 in the endosomal membrane of LCPN cells (**Fig. S5a**). Furthermore, in murine GBM GL261 cells and human GBM U87 MG cells, tNano-S&C exhibited 8.8- and 3.6-fold increase in cellular uptake compared to Nano-S&C (**Fig. S4b,c**), and the STAT3 gene silencing efficacies were 61.2% and 72.3%, respectively (**Fig. S6a,b**). The results were attributable to the high homology of STAT3 gene between humans and mice, confirming the effects of tNano-S&C across different glioma cells.

To evaluate the BBB penetration capacity, an in vitro BBB model was built using a murine bEnd.3 endothelial cell monolayer in transwell inserts, with LCPN cells cultured in the lower chamber. Flow cytometric results indicated that tNano-S&C added in the insert successfully penetrated the monolayer, achieving a remarkable 7.6-fold increase in uptake by LCPN cells compared to non-targeted and free counterparts (Fig. 1h). The results conform to the specific binding of ApoE peptide to LDLRs (including LRP1, LRP2, and LDLR) that are highly expressed in both the BBB and glioma cells [25,31,32].

3.3. Uptake and activation of APCs by tNano-S&C

The cellular uptake and endosome escape of tNano-S&C and tNano-S in murine bone marrow-derived dendritic cells (BMDCs) were also studied using cy5-siSTAT3 as a probe. CLSM images and semi-quantitative analysis of tNano-S&C group displayed ca. 1.6-fold increase in fluorescence intensity compared to tNano-S group at incubation time of 1, 2 and 4 h (Fig. 2a,b). Additionally, tNano-S&C demonstrated superior endosomal escape with decreased co-localization between cy5-siSTAT3 and endosome over time, achieving a reduced Pearson's coefficient of 0.53 at 4 h (Fig. 2c). Notably, the presence of CpG in tNano-S&C significantly enhanced endosomal escape in BMDCs compared to LCPN cells, possibly due to the significantly higher expression of TLR9 in BMDCs (**Fig. S5**), which binds CpG and stimulates

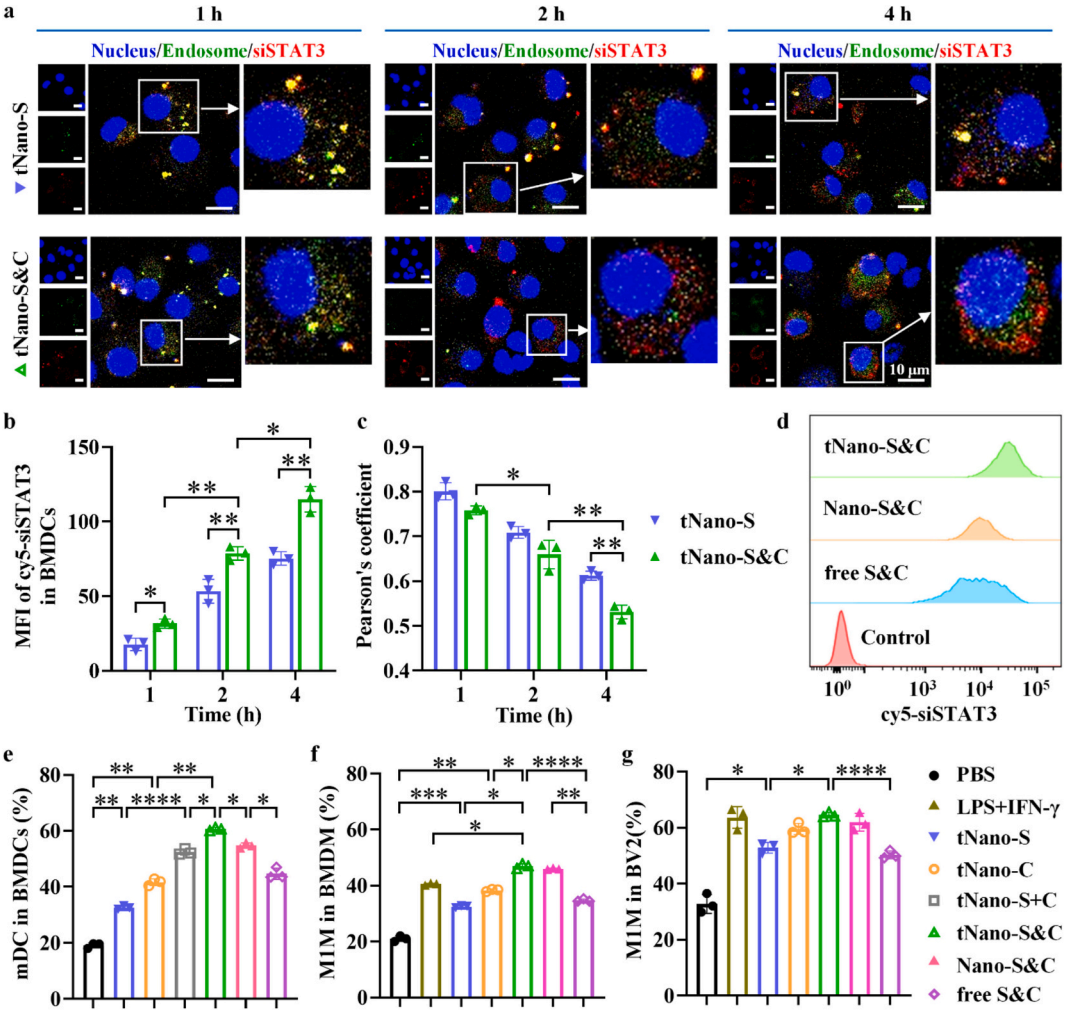

Fig. 2. The uptake and stimulation of APCs by tNano-S&C. a) Uptake and endosomal escape of tNano-S and tNano-S&C in BMDCs (cy5-labeled siSTAT3 as a probe). Scale bars: 10 μm. b) MFI of cy5-siSTAT3 in BMDCs and c) Pearson's coefficient of cy5-siSTAT3 and endosomes as determined by Image J ($n = 3$). d) Flow cytometry analysis of the uptake of tNano-S&C in BMDCs. Percentages of e) mDC in BMDCs, f) M1M in BMDM, and g) M1M in BV2 cells at 24 h incubation with tNano-S&C (siSTAT3: 1 μg mL^{-1}, CpG: 0.5 μg mL^{-1}). PBS and LPS+IFN-γ were as control groups. * $p < 0.05$, ** $p < 0.01$, *** $p < 0.001$, **** $p < 0.0001$.

immune response [33,34].

The overexpression of STAT3 in DCs is known to inhibit their maturation, antigen presentation, and subsequent recruitment and activation of T cells [35]. This dysfunction is a crucial factor for immunosuppressive tumor microenvironment (TME) [21,36]. Flow cytometric analyses confirmed the efficient uptake of tNano-S&C by BMDCs (Fig. 2d), suggesting the capacity of tNano-S&C of activating these immune cells. Compared to the moderate stimulation of DC maturation ($CD11c^+CD80^+CD86^+$, mDC) by tNano-S and tNano-C, tNano-S&C further significantly increased mDC proportion to 60.7% (**, Fig. 2e). tNano-S&C was significantly more potent than Nano-S&C, free S&C and tNano-S+C groups (*). The results demonstrate the critical role of active-targeting in delivering both drugs into the same APC.

Given that glioma-associated macrophages (GAMs), including monocyte-derived macrophages and microglia, comprise major components of the immunosuppressive microenvironment of malignant

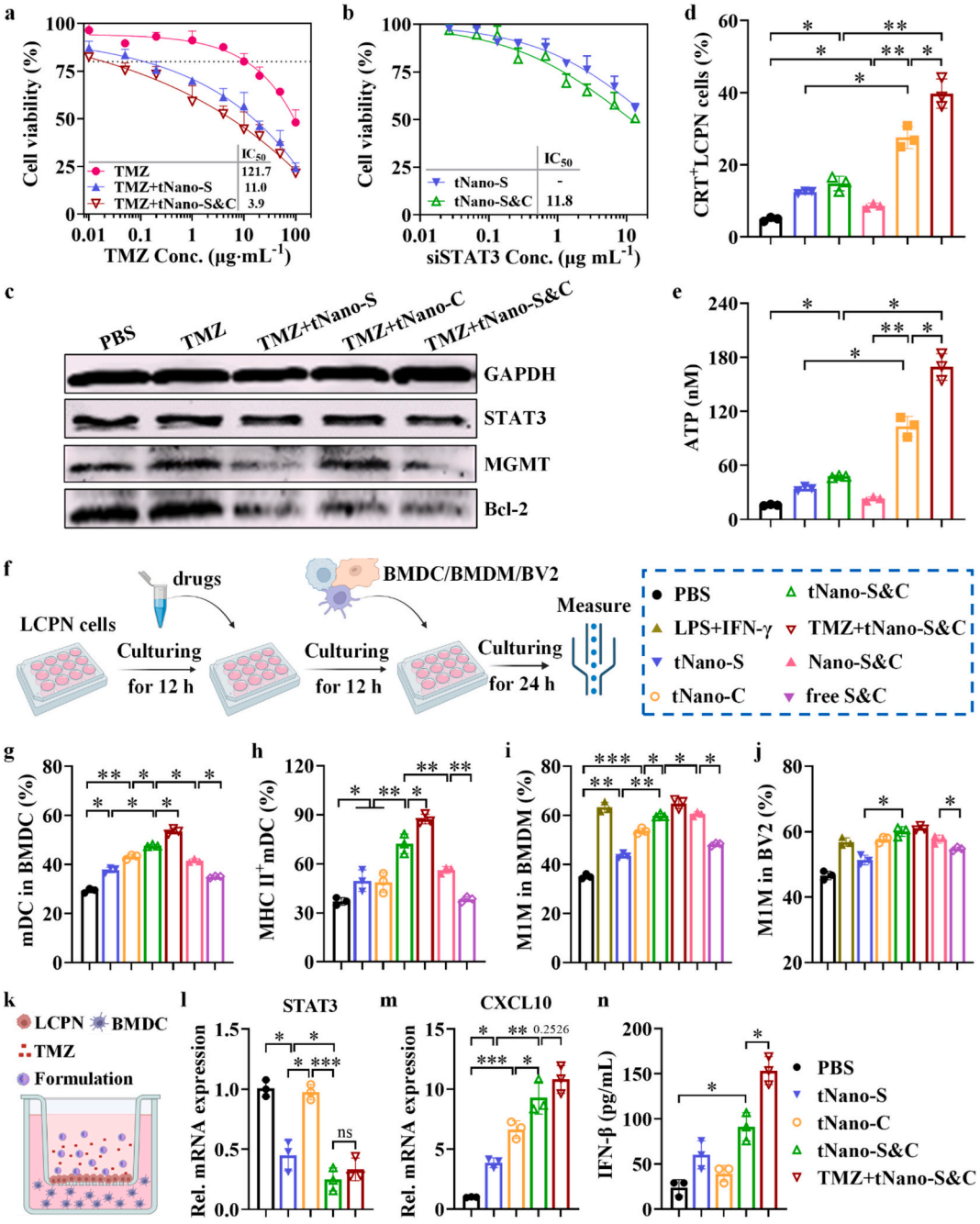

Fig. 3. Combination therapy of tNano-S&C and TMZ synergized in toxicity and ICD of LCPN cells and in the stimulation and chemokine production of APCs. a) MTT assays of LCPN cells incubated with TMZ, TMZ+tNano-S or TMZ+tNano-S&C for 48 h ($n = 3$, TMZ conc.: 0.01–100 μg mL^{-1}, siSTAT3 conc.: 1.33 μg mL^{-1}, CpG conc.: 0.665 μg mL^{-1}). b) Viability of LCPN cells incubated with tNano-S or tNano-S&C for 48 h ($n = 3$, siSTAT3 conc.: 0.02–13.3 μg mL^{-1}, siSTAT3/CpG = 2/1). c) Western blotting of STAT3, MGMT, and Bcl-2 expression in LCPN cells treated with TMZ, TMZ+tNano-S, TMZ+tNano-C or TMZ+tNano-S&C for 48 h. d) Percentages of CRT-positive cells and e) ATP concentration in culture medium of LCPN cells treated with TMZ, TMZ+tNano-S or TMZ+tNano-S&C for 24 h ($n = 3$). f) Schematic of TMZ+tNano-S&C pretreated LCPN cells to stimulate APCs. Percentages of g) mDC in DCs, h) MHC II^+ mDC in mDCs, i) M1M in BMDM, and j) M1M in BV2 cells. A TME-mimicking transwell experiment k) scheme, expression of l) STAT3 mRNA and m) CXCL10 mRNA in BMDCs in lower chamber, and n) IFN-β concentrations in culture medium at 24 h coculturing with TMZ+tNano-S&C and LCPN cells in upper chamber. For c-n, TMZ: 10 μg mL^{-1}, siSTAT3: 1 μg mL^{-1}, CpG: 0.5 μg mL^{-1}, $n = 3$. * $p < 0.05$, ** $p < 0.01$, *** $p < 0.001$.

glioma [37,38], the immunotherapeutic potential of tNano-S&C against GAMs was investigated using BMDMs andBV2 cells. As shown in **Fig. 2f** and **g**, compared to tNano-S and tNano-C, tNano-S&C promoted a greater proportion of pro-inflammatory M1-type macrophages (M1M, $CD11b^{+}F4/80^{+}CD206^{-}$), while reducing M2-type macrophages (M2M, $CD11b^{+}F4/80^{+}CD206^{+}$), which are predominant in GAM populations. The significant decrease in the M2M/M1M ratio (**Fig. S7**) further confirms that tNano-S&C effectively remodels the immunosuppressive TME into immuno-promoting TME.

3.4. Synergistic effect of combination therapy with tNano-S&C and TMZ on cytotoxicity, induction of ICD and stimulation of APCs

The lack of sufficient antigens constitutes another challenge in the immunotherapy of malignant glioma. Consequently, inducing robust tumor cell death is crucial for improving immunogenicity. MTT assay results showed that TMZ, the first-line treatment for glioma, exhibited a half-maximal inhibitory concentration (IC_{50}) of 121.7 μg mL^{-1} against LCPN cells (Fig. 3a). Notably, further combination with tNano-S (TMZ+tNano-S) or tNano-S&C (TMZ+tNano-S&C) drastically sensitized glioma cells to TMZ, resulting in lowered IC_{50} by a factor of 11 and 29, respectively. Considering minimal toxicity for both tNano-S and tNano-S&C at the same siSTAT3 concentration (1.33 μg mL^{-1}) (Fig. 3b), the results indicated a synergistic nature of these combination therapies, with combined index (CI) of 0.16 and 0.14, respectively. Notably, the synergistic cytotoxicity of these two combinations was further confirmed in another murine GBM GL261 cells, showing CI values of 0.27 and 0.09, respectively (**Fig. S6c,d**). Moreover, both combination therapies led to considerable downregulation of O6-methylguanine-DNA methyltransferase (MGMT) and Bcl-2 in LCPN cells contrasting to the increased expression observed in TMZ-only group (Fig. 3c). This indicates that the combination with tNano-S or tNano-S&C could alleviate TMZ resistance and reduce the stemness of glioma cells [21,39].

Additionally, ICD in tumor cell induces the production of calreticulin (CRT) and adenosine triphosphate (ATP), which act as tumor antigens to activate APCs, eliciting tumor-specific cellular immunity [40,41]. The analysis illustrated that TMZ+tNano-S group induced 2.2- to 2.9-fold increase in CRT exposure and 2.8- to 4.5-fold increase in ATP secretion compared to tNano-S and TMZ monotherapies, respectively. Remarkably, compared to TMZ+tNano-S group, TMZ+tNano-S&C therapy further increased CRT and ATP expression by 1.4- to 1.6-fold (Fig. 3d,e), reflecting its superior capacity for ICD induction. Consequently, TMZ+tNano-S&C was selected for further investigations on in vitro immune stimulation and in vivo anti-tumor therapy.

To elucidate the stimulatory effects of ICD on APCs, DCs or macrophages were co-cultured with LCPN cells that were pretreated with tNano-S&C formulations and the results were analyzed using flow cytometry (Fig. 3f). The results revealed a significant increase in the mDC proportion in TMZ+tNano-S&C group, demonstrating the following hierarchy in effectiveness: tNano-S < tNano-C < tNano-S&C < TMZ+tNano-S&C (Fig. 3g). Moreover, both tNano-S&C and TMZ+tNano-S&C significantly upregulated MHC II molecules on mDCs (Fig. 3h), which enables antigen presentation to $CD4^{+}$ T cells. Similarly, polarization studies of BMDM and BV2 cells after co-culture further corroborated the highest stimulatory effect of TMZ+tNano-S&C treatment, promoting the M1M phenotype (Fig. 3i,j), known for its antitumor activity.

We employed a tumor-mimicking transwell model (Fig. 3k) to further elucidate the molecular mechanisms underlying this immune response. qRT-PCR analysis of the DCs in the lower chamber revealed that antigens derived from LCPN cells treated with tNano-S&C or TMZ+tNano-S&C as well as the nanoformulations could traverse the inset membrane and significantly downregulated STAT3 mRNA and upregulated CXCL10 mRNA in BMDCs (Fig. 3l,m). The upregulation of CXCL10 in glioma tissues may reflect changes in TME, such as the interactions between tumor cells and immune cells [12]. Glioma cells by releasing specific signaling molecules can induce CXCL10 expression in DCs, which is a crucial chemokine for attracting effector T cells, such as $CD8^{+}$ T cells, to migrate to the tumor sites [42]. This chemokine plays a vital role in orchestrating an effective anti-glioma immune responses and surveillance in vivo. Interestingly, TMZ+tNano-S&C treatment enhanced the secretion of IFN-β by BMDCs (Fig. 3n) by 1.7- to 3.9-fold compared to tNano-S&C and other control groups, indicating the crucial role of this treatment in the cross-presentation of tumor antigens and activation of anti-glioma immune responses [43].

3.5. Biodistribution studies of tNano-S&C in orthotopic LCPN-bearing mice

The orthotopic murine LCPN-bearing model represents an aggressive tumor model that is largely refractory to ICB such as anti-PD-1 and anti-CTLA-4 [25], thereby resembling the clinical scenario in malignant glioma patients. This model was employed to study the biodistribution of tNano-S&C (using cy7-labeled CpG as a probe) after a single intravenous (i.v.) injection. In vivo imaging revealed a significant brain accumulation of tNano-S&C at 4, 8 and 12 h post-injection, achieving 2.7- and 4.2-fold higher levels compared to both Nano-S&C and free S&C at 12 h (Fig. 4a). Ex vivo imaging confirmed ca. 4-fold increased deposition of tNano-S&C in tumor-bearing brain tissue and 2-fold in cervical lymph nodes (CLNs) compared to Nano-S&C (Fig. 4b). Besides, the nanoformulations displayed reduced accumulation in the kidneys, livers and lungs compared to free S&C (Fig. 4c), indicating a slower metabolic clearance of CpG when encapsulated within polymersomes. Notably, glioma cells of tNano-S&C group exhibited 3.5-fold greater MFI than that of normal brain cells (**, Fig. 4d), demonstrating the glioma-targeting capability of tNano-S&C in vivo. Furthermore, tNano-S&C also accumulated significantly more in CLNs and spleen than control formulations, pointing to its potential role in stimulating local and systemic immune responses.

Subsequently, the uptake of tNano-S&C by immune cells within tumor, CLNs and spleen was analyzed following the preparation of single cell suspension. Flow cytometry analysis revealed that about 3.1% total cells in tumor issues endocytosed tNano-S&C, with about 42% of these being $CD45^{-}$ cells (mainly glioma cells) and 58% $CD45^{+}$ cells (immune cells) (Fig. 4e). Among $CD45^{+}$ cells, 54% of tNano-S&C was delivered to DCs and 29% to macrophages. DCs are the most powerful professional APCs in TME, and can migrate to CLNs to present tumor antigens to T cells. Macrophages in glioma mainly present MHC II molecules, interacting directly with $CD4^{+}$ T cells in brain TME [44]. Interestingly, compared to Nano-S&C and free S&C groups, tNano-S&C group exhibited not only significantly increased deposition in DCs and macrophages, but also enhanced proliferation of these immune cells (Fig. 4f), probably due to the production of chemokines. Similar trends were found in the CLNs and spleen concerning tNano-S&C localization within immune cells (Fig. 4g,h). These results indicate that tNano-S&C is not only capable of targeting glioma but also stimulating both local and systemic anti-glioma immune responses in LCPN models. This finding is paramount, as insufficient antigens and poor accumulation in immune organs have long been considered as major bottlenecks for the effective therapy of malignant glioma [18,45].

3.6. Immunotherapy of LCPN mice with combination therapy of tNano-S&C and TMZ

Encouraged by the notable accumulation of tNano-S&C in glioma tumors and immune cells in vivo, in the following study, we investigated its anti-glioma efficacy alone or in combination with TMZ. In a preliminary experiment, orthotopic LCPN models were i.v. injected with tNano-S&C on days 3, 5, 7, 17, and 19 at two doses ($n = 4$). The results showed that PBS treated mice exhibited drastic body weight loss starting on day 15 and succumbed shortly thereafter, while tNano-S&C (each dose with siSTAT3: 2 mg kg^{-1}, siSTAT3/CpG = 2/1) significantly

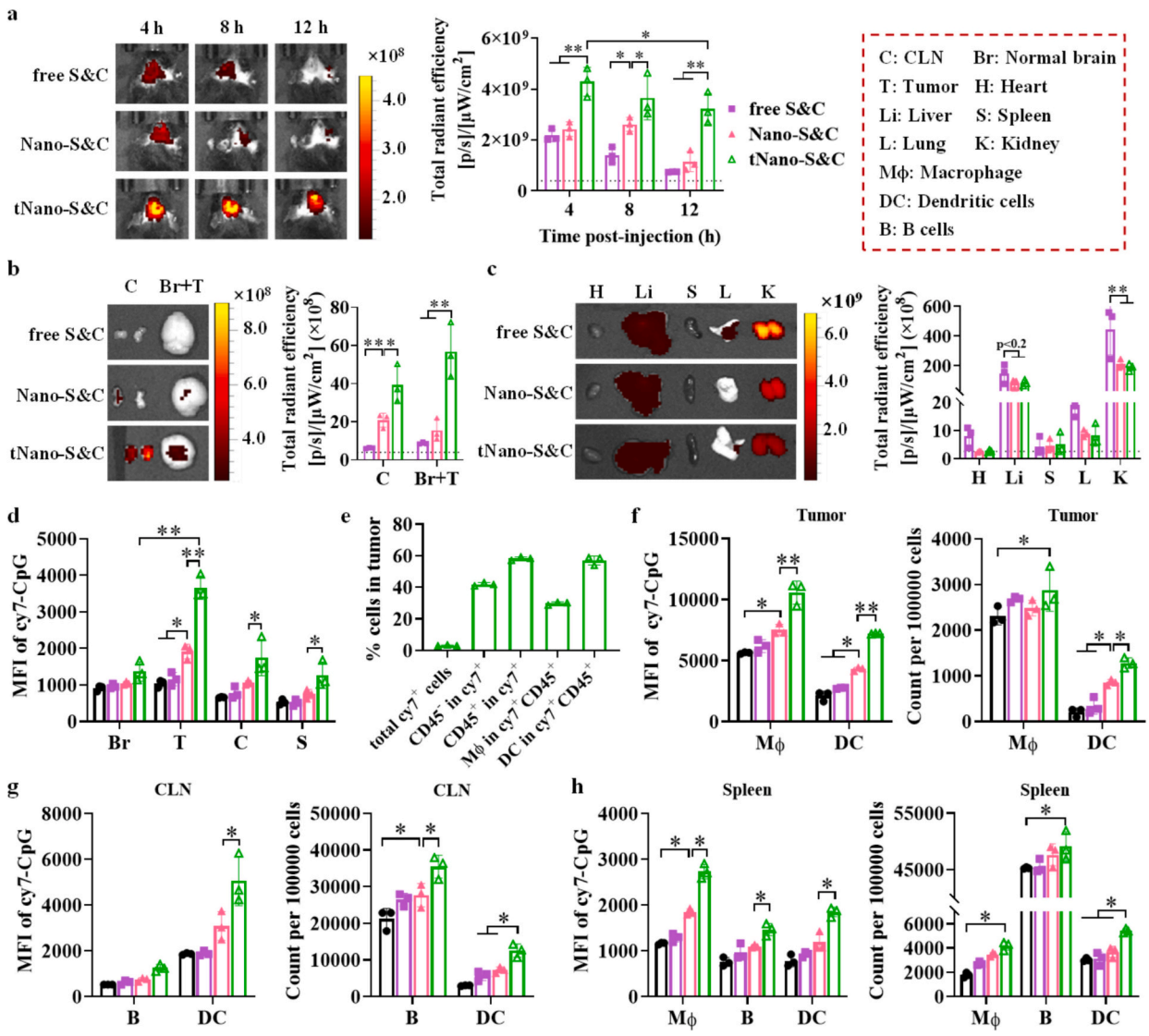

Fig. 4. Biodistribution studies of tNano-S&C (0.8 *wt.*% cy7-CpG as a probe) in orthotopic murine LCPN mice following a single i.v. injection ($n = 3$). a) In vivo imaging and semiquantification of the brain. Ex vivo imaging and semiquantification of b) brain and CLNs, and c) major organs at 12 h post injection. d) MFI of tNano-S&C uptake by single cell suspension of normal brain, tumor, CLNs and spleen. e) Percentages of cy7-CpG$^+$ cells in total tumor tissue cells, CD45$^-$ cells (mainly tumor cells) and CD45$^+$ cells (mainly immune cells) in total cy7-CpG$^+$ cells, as well as macrophages (Mϕ) and DCs in cy7-CpG$^+$CD45$^+$ cells. MFI of cy7 in APCs and total number of these APCs in f) tumor, g) CLNs and h) spleen. * $p < 0.05$, ** $p < 0.01$.

inhibited glioma progression and prolonged the median survival time (MST) to 49 days in a dose-dependent manner (**Fig. S8**). In another independent in vivo experiment with the same dosing scheme (Fig. 5a, $n = 6$), tNano-S&C identically demonstrated glioma suppression ability with MST of 50 days. The results showed that treatments with free S&C and nanoformulations all delayed disease progression, with almost constant body weight until day 22 (Fig. 5b) and significantly extended (MST compared to PBS group (21 d): free S&C (28 d), Nano-S&C (36 d), tNano-S (32 d), tNano-C (38 d), tNano-S+C (42 d), and tNano-S&C (50 d) (Fig. 5c). The significantly extended MST in the tNano-S&C group confirms its active targeting capacity in orthotopic glioma models. Notably, tNano-S&C also testified anti-glioma efficacy in orthotopic GL261 models, with slightly weaker capability in inhibiting tumor progression and extending MST (45 days, **Fig. S9**).

Further combined TMZ was administered orally for five consecutive days at 40 mg kg^{-1}, reflecting the standard clinical dosage [46]. This combination therapy displayed a remarkable extension of lifespan, yielding an MST of 58 days (*), with 1 out of 6 LCPN mice remaining tumor-free for over 300 d (Fig. 5c). Hematoxylin-eosin (H&E) staining of tumor-containing brain slices harvested on day 23 demonstrated that TMZ+tNano-S&C group had the smallest tumors, with extensive tumor cell apoptosis and necrosis (Fig. 5d). In contrast, TMZ monotherapy exhibited limited efficacy, yielding an MST of 26 d (Fig. 5e, f). Despite being first-line drug for glioma, TMZ is often ineffective for many malignant glioma patients due to inherent insensitivity or acquired resistance. The comparison of survival curves indicates that TMZ+tNano-S&C group enhanced the efficacy observed in the two monotherapies, extending MST in a synergistic manner (Fig. 5c,f). This enhanced efficacy correlates with the great downregulation of MGMT and Bcl-2 (Fig. 3c), both of which are implicated in TMZ resistance, thereby enhancing glioma cell sensitivity to this chemotherapeutic agent. Moreover, in contrast to the strong anti-GBM efficacy of tNano-C alone compared to tNano-S alone, which is attributable to tNano-C's superior immune activation capability, TMZ+tNano-C group (MST: 35 d) showed slightly reduced therapeutic efficacy compared to TMZ+tNano-S group (MST: 37 d). This diminished efficacy can be attributed to the inability of tNano-C to downregulate the TMZ-induced elevated expression of MGMT (Fig. 3c) and PD-L1 in LCPN cells (**Fig. S10**), both of which

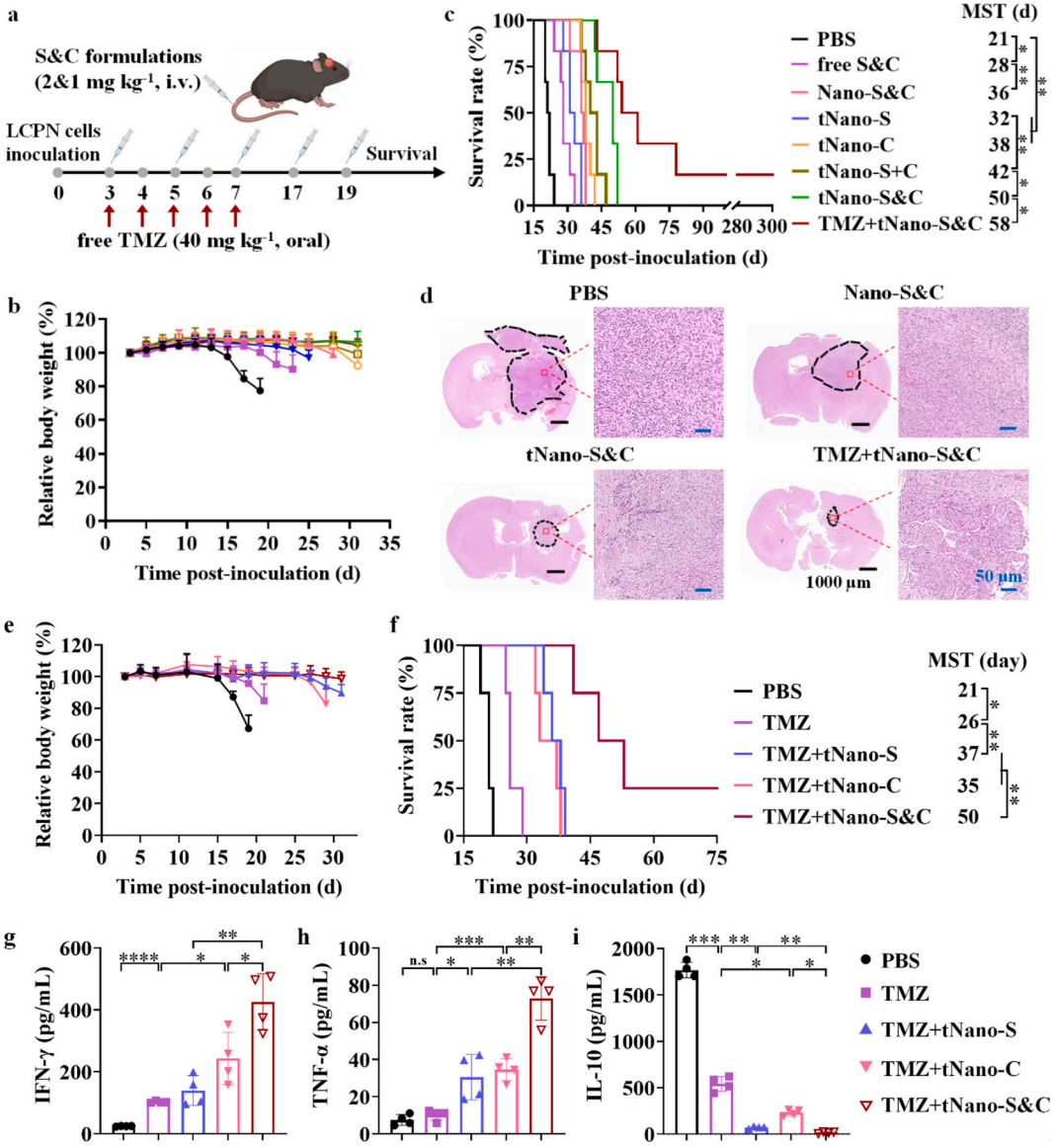

Fig. 5. Treatment with tNano-S&C and TMZ+tNano-S&C in orthotopic LCPN mice. a) Treatment scheme. b) Relative body weight and c) survival curves of the mice treated with tNano-S&C and TMZ+tNano-S&C and other control groups ($n = 6$). d) H&E staining of tumor-containing brain slics of LCPN mice on day 23. e) Relative body weight and f) survival curves of the mice treated with TMZ and TMZ+tNano-S&C. Plasma concentrations of g) IFN-γ, h) TNF-α and i) IL-10 on day 7 ($n = 4$). * $p < 0.05$, ** $p < 0.01$, *** $p < 0.001$, **** $p < 0.0001$.

contribute to TMZ resistance and immune suppression in GBM therapy, respectively. These results underscore the importance of strategic codelivery of siSTAT3 and CpG via polymersomes in enhancing the therapeutic outcomes of GBM when combined with TMZ.

Furthermore, plasma levels of proinflammatory cytokines, including interferon gamma (IFN-γ) and tumor necrosis factor α (TNF-α) were augmented by 1.8- to 6.6-fold in TMZ+tNano-S&C group compared to TMZ, TMZ+tNano-S and TMZ+tNano-C groups. Concurrently, the immunosuppressive cytokine interleukin-10 (IL-10) was significantly decreased by factors of 20, 3 and 10, respectively (Fig. 5g-i). These results highlight the important role of down-regulation of STAT3 in reversing the immunosuppressive microenvironment prevalent in glioma. Collectively, these results affirm the robust anti-glioma capacities of TMZ+tNano-S&C, demonstrating its potential to effectively reprogram the immune landscape while sensitizing orthotopic glioma cells to TMZ.

3.7. Immunological analysis of orthotopic LCPN mice treated with TMZ+tNano-S&C

The immune stimulatory mechanism of tNano-S&C and TMZ+tNano-S&C in orthotopic LCPN mice was elucidated. Mice were i. v. injected with three times of tNano-S&C or in combination with five oral TMZ doses, and 24 h after last dose the immune cells in tumor, CLNs and spleen were harvested and analyzed (Fig. 6a). On day 14, tumor inhibition rates were observed at 67% and 78% for tNano-S&C and TMZ+tNano-S&C, respectively (**Fig. S11a,b**). Immunological analysis of TME revealed that tNano-S&C and TMZ+tNano-S&C treatments resulted in a 4.1-fold increase in total DC contents ($CD11c^+$), and 4.4- to 6.0-fold increase in mDC contents ($CD11c^+CD80^+CD86^+$) compared to control formulations (Fig. 6b, c). Notably, TMZ+tNano-S&C group exhibited significantly enhanced tumor infiltration of T cells, with increases ranging from 1.4- to 4.6-fold in total T cells ($CD3^+$), $CD8^+$T cells ($CD3^+CD8^+$) and helper T cells ($CD4^+$T, $CD3^+CD4^+$) compared to tNano-S&C and other control groups (Fig. 6d-f). Moreover, TMZ+tNano-

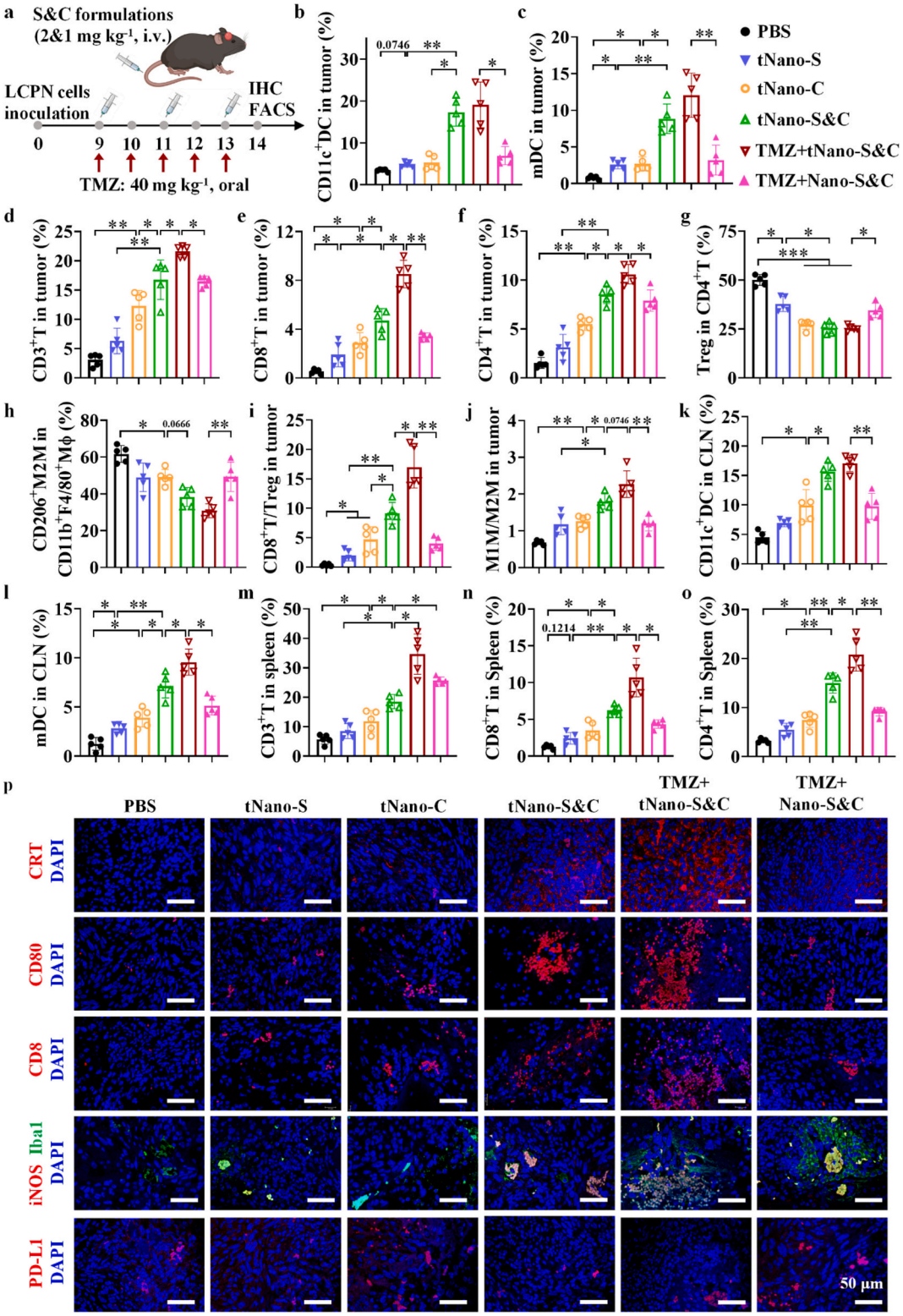

Fig. 6. Immunological analysis of orthotopic LCPN mice treated with tNano-S&C and TMZ+tNano-S&C ($n = 6$). a) Workflow. Percentages of b) DCs, c) mDCs, d) $CD3^+$T, e) $CD8^+$T, f) $CD4^+$T, g) Treg in $CD4^+$T, and h) $CD206^+$ M2M out of total Mϕ in tumor. Ratios of i) $CD8^+$T/Treg and j) M1M/M2M in tumor. Percentages of k) DCs and l) mDCs in CLN. Percentages of m) $CD3^+$T, n) $CD8^+$T and o) $CD4^+$T cells in spleen ($n = 5$). p) Immuno-histochemical staining of CRT^+ cells, DCs ($CD80^+$), CTLs ($CD8^+$), M1M and PD-$L1^+$cells in tumors on day 14 ($n = 1$). Scale bars: 50 μm. * $p < 0.05$, ** $p < 0.01$, *** $p < 0.001$, **** $p < 0.0001$.

S&C significantly reduced the proportions of immunosuppressive cells, specifically regulatory T cells (Tregs, $CD3^+CD4^+foxp3^+$) and M2 phenotype macrophages (M2M, $CD11b^+CD206^+$), by a factor of 2 compared to PBS group (Fig. 6g,h). This shift led to significant increases in the ratios of $CD8^+$T/Treg and M1M/M2M in the TME (Fig. 6i,j), demonstrating their capacity to effectively reprogram the immunosuppressive TME. It is known that the refractoriness of malignant glioma is partially related to its immunosuppressive microenvironment.

Given the previously noted accumulation of tNano-S&C in the CLNs and spleen, we further analyzed the activation of local and systemic immunity in these tissues. CLNs are critical for immune surveillance and regulation in orthotopic glioma, in which APCs (especially DCs) present glioma antigens to T cells. Results displayed that, while the total DCs was comparable, TMZ+tNano-S&C treatment induced a significantly greater number of mDCs in CLNs than tNano-S&C and other controls (Fig. 6k,l). In the spleen, TMZ+tNano-S&C led to a significant increase in the percentages of $CD3^+$T, $CD4^+$T and $CD8^+$T cells compared to tNano-S&C and other groups (Fig. 6m-o), illustrating a robust systemic T cell response. Notably, mice receiving TMZ+tNano-S&C treatment maintained normal spleen weights, in contrast to the splenomegaly observed in tNano-C and tNano-S&C groups (**Fig. S11c**). Furthermore, both tNano-S&C and TMZ+tNano-S&C increased the production of TNF-α and IFN-γ, alongside nearly undetectable IL-10 levels (**Fig. S11d-f**).

Immunohistochemical (IHC) staining of brain tumor slices validated that tNano-S&C induced high levels of ICD (CRT), APC activation (mDCs, CD80), $CD8^+$T cells infiltration (CD8), and $iNOS^+$ macrophage (M1M) compared to control groups. As expected, TMZ+tNano-S&C further substantially amplified these markers (Fig. 6p). Remarkably, both tNano-S&C and TMZ+tNano-S&C resulted in very low levels of immunosuppressive PD-$L1^+$cells and M2M. Additionally, these immune cells were predominantly located within and around the tumors, with minimal presence in normal brain tissue (**Fig. S12**), indicating favorable safety profile of the treatments.

4. Conclusion

We have demonstrated that systemic administration of ApoE-targeted nano-polymersomes co-loading siSTAT3 and CpG ODN (tNano-S&C) affords markedly enhanced drug accumulation in the malignant glioma tumors and associated immune organs, resulting in effective knockdown of STAT3 and reversal of immunosuppressive TME characteristic of malignant gliomas. Of note, tNano-S&C greatly sensitizes glioma cells to TMZ therapy and amplifies the efficacy of chemo-immunotherapy in highly malignant murine LCPN glioma models. This observed therapeutic synergy has led to significant survival benefits, with some mice achieving complete tumor regression, underscoring a powerful activation of anti-glioma immunity. To the best of our knowledge, this represents the first report of systemic co-administration of siSTAT3 and CpG via brain-targeted polymersomes for the treatment of malignant glioma. Our findings not only illuminate a novel strategy to enhance chemo-immunotherapy but also provide critical insights into the mechanisms by which ICD and the reprogramming of the immunosuppressive microenvironment can be achieved. This study paves a new way to enhance the chemo-immunotherapy of malignant glioma.

CRediT authorship contribution statement

Songsong Zhao: Writing – original draft, Methodology, Investigation, Formal analysis, Data curation, Conceptualization. **Zhiwei Sun:** Investigation, Formal analysis. **Mingyu Xia:** Investigation, Formal analysis. **Beibei Guo:** Investigation, Formal analysis. **Yanyi Qu:** Investigation, Formal analysis. **Jingyi Wang:** Investigation, Formal analysis. **Zhiyuan Zhong:** Writing – review & editing, Supervision, Resources, Conceptualization. **Fenghua Meng:** Writing – review & editing, Validation, Supervision, Project administration, Funding acquisition, Conceptualization.

Declaration of competing interest

The authors declare that they have no known competing financial interests or personal relationships that could have appeared to influence the work reported in this paper.

Acknowledgement

This work is supported by research grants from the National Natural Science Foundation of China (NSFC 52473142, 52033006) and the National Key R&D Program of China (2022YFA1206000). The authors thank Biorender.com for the assistance in illustrations.

Appendix A. Supplementary data

Supplementary data to this article can be found online at https://doi.org/10.1016/j.jconrel.2025.113764.

Data availability

Data will be made available on request.

References

[1] A.C. Tan, D.M. Ashley, G.Y. López, M. Malinzak, H.S. Friedman, M. Khasraw, Management of glioblastoma: state of the art and future directions, CA Cancer J. Clin. 70 (2020) 299–312, https://doi.org/10.3322/caac.21613.
[2] C. Horbinski, T. Berger, R.J. Packer, P.Y. Wen, Clinical implications of the 2021 edition of the WHO classification of central nervous system tumours, Nat. Rev. Neurol. 18 (2022) 515–529, https://doi.org/10.1038/s41582-022-00679-w.
[3] Y. Yan, S. Zhou, X. Chen, Q. Yi, S. Feng, Z. Zhao, Y. Liu, Q. Liang, Z. Xu, Z. Li, L. Sun, Suppression of ITPKB degradation by Trim25 confers TMZ resistance in glioblastoma through ROS homeostasis, Signal Transduct. Target. Ther. 9 (2024) 58, https://doi.org/10.1038/s41392-024-01763-x.
[4] T.I. Janjua, P. Rewatkar, A. Ahmed-Cox, I. Saeed, F.M. Mansfeld, R. Kulshreshtha, T. Kumeria, D.S. Ziegler, M. Kavallaris, R. Mazzieri, A. Popat, Frontiers in the treatment of glioblastoma: past, present and emerging, Adv. Drug Deliv. Rev. 171 (2021) 108–138, https://doi.org/10.1016/j.addr.2021.01.012.
[5] M.S. Tomar, A. Kumar, C. Srivastava, A. Shrivastava, Elucidating the mechanisms of Temozolomide resistance in gliomas and the strategies to overcome the resistance, Biochim. Biophys. Acta 1876 (2021) 188616, https://doi.org/10.1016/j.bbcan.2021.188616.
[6] X. Meng, Y. Zhao, B. Han, C. Zha, Y. Zhang, Z. Li, P. Wu, T. Qi, C. Jiang, Y. Liu, J. Cai, Dual functionalized brain-targeting nanoinhibitors restrain temozolomide-resistant glioma via attenuating EGFR and MET signaling pathways, Nat. Commun. 11 (2020) 594, https://doi.org/10.1038/s41467-019-14036-x.
[7] J.X. Yin, X. Ge, F.S. Ding, L.G.J. He, K.Y. Song, Z.M. Shi, Z.H. Ge, J.X. Zhang, J. Ji, X.F. Wang, N.W. Zhao, C.J. Shu, F. Lin, Q.H. Wang, Q.G. Zhou, Y.D. Cao, W.T. Liu, D. Ye, J.N. Rich, X.X. Wang, Y.P. You, X. Qian, Reactivating PTEN to impair glioma stem cells by inhibiting cytosolic iron-sulfur assembly, Sci. Transl. Med. 16 (2024) eadg5553, https://doi.org/10.1126/scitranslmed.adg5553.
[8] K. Lin, S.E. Gueble, R.K. Sundaram, E.D. Huseman, R.S. Bindra, S.B. Herzon, Mechanism-based design of agents that selectively target drug-resistant glioma, Science 377 (2022) 502–511, https://doi.org/10.1126/science.abn7570.
[9] J.W. Cui, X. Wang, J.E. Li, A.R. Zhu, Y.M. Guo, L.Q. Di, R.N. Wang, Immune exosomes loading self-assembled Nanomicelles traverse the blood-brain barrier for chemo-immunotherapy against glioblastoma, ACS Nano 17 (2023) 1464–1484, https://doi.org/10.1021/acsnano.2c10219.
[10] X. Wang, L. Ye, W. He, C. Teng, S. Sun, H. Lu, S. Li, L. Lv, X. Cao, H. Yin, W. Lv, H. Xin, In situ targeting nanoparticles-hydrogel hybrid system for combined chemo-immunotherapy of glioma, J. Control. Release 345 (2022) 786–797, https://doi.org/10.1016/j.jconrel.2022.03.050.
[11] G. Agliardi, A.R. Liuzzi, A. Hotblack, D. De Feo, N. Núñez, C.L. Stowe, E. Friebel, F. Nannini, L. Rindlisbacher, T.A. Roberts, R. Ramasawmy, I.P. Williams, B. M. Siow, M.F. Lythgoe, T.L. Kalber, S.A. Quezada, M.A. Pule, S. Tugues, K. Straathof, B. Becher, Intratumoral IL-12 delivery empowers CAR-T cell immunotherapy in a pre-clinical model of glioblastoma, Nat. Commun. 12 (2021) 444, https://doi.org/10.1038/s41467-020-20599-x.
[12] J. Zhang, C. Chen, A. Li, W. Jing, P. Sun, X. Huang, Y. Liu, S. Zhang, W. Du, R. Zhang, Y. Liu, A. Gong, J. Wu, X. Jiang, Immunostimulant hydrogel for the inhibition of malignant glioma relapse post-resection, Nat. Nanotechnol. 16 (2021) 538–548, https://doi.org/10.1038/s41565-020-00843-7.
[13] S. Zhou, Y. Huang, Y. Chen, Y. Liu, L. Xie, Y. You, S. Tong, J. Xu, G. Jiang, Q. Song, N. Mei, F. Ma, X. Gao, H. Chen, J. Chen, Reprogramming systemic and local immune function to empower immunotherapy against glioblastoma, Nat. Commun. 14 (2023) 435, https://doi.org/10.1038/s41467-023-35957-8.
[14] E. Memari, D. Khan, R. Alkins, B. Helfield, Focused ultrasound-assisted delivery of immunomodulating agents in brain cancer, J. Control. Release 367 (2024) 283–299, https://doi.org/10.1016/j.jconrel.2024.01.034.
[15] R. Ursu, S. Taillibert, C. Banissi, E. Vicaut, O. Bailon, E. Le Rhun, J.S. Guillamo, D. Psimaras, A. Tibi, A. Sacko, A. Marantidou, C. Belin, A.F. Carpentier, Immunotherapy with CpG-ODN in neoplastic meningitis: a phase I trial, Cancer Sci. 106 (2015) 1212–1218, https://doi.org/10.1200/jco.2013.31.15_suppl.3065.
[16] M. Lim, M. Weller, A. Idbaih, J. Steinbach, G. Finocchiaro, R. Raval, L. Ashby, G. Ansstas, J. Baehring, J. Taylor, J. Honnorat, K. Petrecca, F. De Vos, A. Wick, A. Sumrall, M. Roberts, R. Slepetis, D. Warad, M. Lee, D. Reardon, A. Omuro, Phase III trial of chemoradiotherapy with temozolomide plus nivolumab or placebo for

newly diagnosed glioblastoma with methylated MGMT promoter, Neuro-Oncology 24 (2022) 1935–1949, https://doi.org/10.1093/neuonc/noac116.
[17] D.A. Reardon, A. Desjardins, J.J. Vredenburgh, D.M. O'Rourke, D.D. Tran, K. L. Fink, L.B. Nabors, G. Li, D.A. Bota, R.V. Lukas, L.S. Ashby, J.P. Duic, M. M. Mrugala, S. Cruickshank, L. Vitale, Y. He, J.A. Green, M.J. Yellin, C.D. Turner, T. Keler, T.A. Davis, J.H. Sampson, Rindopepimut with bevacizumab for patients with relapsed EGFRvIII-expressing glioblastoma (ReACT): results of a double-blind randomized phase II trial, Clin. Cancer Res. 26 (2020) 1586–1594, https://doi.org/10.1158/1078-0432.ccr-18-1140.
[18] J.H. Sampson, M.D. Gunn, P.E. Fecci, D.M. Ashley, Brain immunology and immunotherapy in brain tumours, Nat. Rev. Cancer 20 (2019) 12–25, https://doi.org/10.1038/s41568-019-0224-7.
[19] F. Hameedat, B.B. Mendes, J. Conniot, L.D. Di Filippo, M. Chorilli, A. Schroeder, J. Conde, F. Sousa, Engineering nanomaterials for glioblastoma nanovaccination, Nat. Rev. Mater. 9 (2024) 628–642, https://doi.org/10.1038/s41578-024-00684-z.
[20] S. Li, C. Wang, J. Chen, Y. Lan, W. Zhang, Z. Kang, Y. Zheng, R. Zhang, J. Yu, W. Li, Signaling pathways in brain tumors and therapeutic interventions, Signal Transduct. Target. Ther. 8 (2023) 8, https://doi.org/10.1038/s41392-022-01260-z.
[21] L. Pang, M. Dunterman, S. Guo, F. Khan, Y. Liu, E. Taefi, A. Bahrami, C. Geula, W. H. Hsu, C. Horbinski, C.D. James, P. Chen, Kunitz-type protease inhibitor TFPI2 remodels stemness and immunosuppressive tumor microenvironment in glioblastoma, Nat. Immunol. 24 (2023) 1654–1670, https://doi.org/10.1038/s41590-023-01605-y.
[22] J. Wang, Z. Huang, L. Ji, C. Chen, Q. Wan, Y. Xin, Z. Pu, K. Li, J. Jiao, Y. Yin, Y. Hu, L. Gong, R. Zhang, X. Yang, X. Fang, M. Wang, B. Zhang, J. Shao, J. Zou, SHF acts as a novel tumor suppressor in glioblastoma Multiforme by disrupting STAT3 dimerization, Adv. Sci. 9 (2022) e2200169, https://doi.org/10.1002/advs.202200169.
[23] Y. Li, Z. Song, Q. Han, H. Zhao, Z. Pan, Z. Lei, J. Zhang, Targeted inhibition of STAT3 induces immunogenic cell death of hepatocellular carcinoma cells via glycolysis, Mol. Oncol. 16 (2022) 2861–2880, https://doi.org/10.1002/1878-0261.13263.
[24] Y. Lee, J. Shinn, C. Xu, H.E. Dobson, N. Neamati, J.J. Moon, Hyaluronic acid-bilirubin nanomedicine-based combination chemoimmunotherapy, Nat. Commun. 14 (2023) 4771, https://doi.org/10.1038/s41467-023-40270-5.
[25] J. Wei, D. Wu, S. Zhao, Y. Shao, Y. Xia, D. Ni, X. Qiu, J. Zhang, J. Chen, F. Meng, Z. Zhong, Immunotherapy of malignant glioma by noninvasive administration of TLR9 agonist CpG Nano-Immunoadjuvant, Adv. Sci. 9 (2022) 2103689, https://doi.org/10.1002/advs.202103689.
[26] J. Wei, D. Wu, Y. Shao, B. Guo, J. Jiang, J. Chen, J. Zhang, F. Meng, Z. Zhong, ApoE-mediated systemic nanodelivery of granzyme B and CpG for enhanced glioma immunotherapy, J. Control. Release 347 (2022) 68–77, https://doi.org/10.1016/j.jconrel.2022.04.048.
[27] D.M. Hossain, C. Dos Santos, Q. Zhang, A. Kozlowska, H. Liu, C. Gao, D. Moreira, P. Swiderski, A. Jozwiak, J. Kline, S. Forman, R. Bhatia, Y.H. Kuo, M. Kortylewski, Leukemia cell-targeted STAT3 silencing and TLR9 triggering generate systemic antitumor immunity, Blood 123 (2014) 15–25, https://doi.org/10.1182/blood-2013-07-517987.
[28] X. Zhao, Z. Zhang, D. Moreira, Y.L. Su, H. Won, T. Adamus, Z. Dong, Y. Liang, H. H. Yin, P. Swiderski, R.K. Pillai, L. Kwak, S. Forman, M. Kortylewski, B cell lymphoma immunotherapy using TLR9-targeted oligonucleotide STAT3 inhibitors, Mol. Ther. 26 (2018) 695–707, https://doi.org/10.1016/j.ymthe.2018.01.007.
[29] W. Ngamcherdtrakul, M. Reda, M.A. Nelson, R. Wang, H.Y. Zaidan, D.S. Bejan, N. H. Hoang, R.S. Lane, S.W. Luoh, S.A. Leachman, G.B. Mills, J.W. Gray, A.W. Lund, W. Yantasee, In situ tumor vaccination with nanoparticle co-delivering CpG and STAT3 siRNA to effectively induce whole-body antitumor immune response, Adv. Mater. 33 (2021) e2100628, https://doi.org/10.1002/adma.202100628.
[30] T. Adamus, C.Y. Hung, C. Yu, E. Kang, M. Hammad, L. Flores, S. Nechaev, Q. Zhang, J.M. Gonzaga, K. Muthaiyah, P. Swiderski, K.S. Aboody, M. Kortylewski, Glioma-targeted delivery of exosome-encapsulated antisense oligonucleotides using neural stem cells, Mol. Ther. Nucl. Acids 27 (2022) 611–620, https://doi.org/10.1016/j.omtn.2021.12.029.
[31] Y. Zhang, H. Ma, L. Li, C. Sun, C. Yu, L. Wang, D. Xu, X. Song, R. Yu, Dual-targeted novel temozolomide nanocapsules encapsulating siPKM2 inhibit aerobic glycolysis to sensitize glioblastoma to chemotherapy, Adv. Mater. 36 (2024) e2400502, https://doi.org/10.1002/adma.202400502.
[32] W. He, X. Li, M. Morsch, M. Ismail, Y. Liu, F.U. Rehman, D. Zhang, Y. Wang, M. Zheng, R. Chung, Y. Zou, B. Shi, Brain-targeted codelivery of Bcl-2/Bcl-xl and Mcl-1 inhibitors by biomimetic nanoparticles for orthotopic glioblastoma therapy, ACS Nano 16 (2022) 6293–6308, https://doi.org/10.1021/acsnano.2c00320.
[33] X. Zhao, Y. Dong, J. Zhang, C. Chen, L. Gao, C. Shi, Z. Fu, M. Han, C. Tang, P. Sun, Z. Yang, C. Zhang, K. Zhao, X. Jiang, Reversing immune evasion using a DNA nano-orchestrator for pancreatic cancer immunotherapy, Acta Biomater. 166 (2023) 512–523, https://doi.org/10.1016/j.actbio.2023.05.001.
[34] L. Wang, C. Zhang, J. Zhao, Z. Zhu, J. Wang, W. Fan, W. Jia, Biomimetic targeting nanoadjuvants for sonodynamic and chronological multi-immunotherapy against holistic biofilm-related infections, Adv. Mater. 36 (2024) e2308110, https://doi.org/10.1002/adma.202308110.
[35] A. Ou, M. Ott, D. Fang, A.B. Heimberger, The role and therapeutic targeting of JAK/STAT signaling in glioblastoma, Cancers 13 (2021) 437, https://doi.org/10.3390/cancers13030437.
[36] W. Yuan, Q. Zhang, D. Gu, C. Lu, D. Dixit, R.C. Gimple, Y. Gao, J. Gao, D. Li, D. Shan, L. Hu, L. Li, Y. Li, S. Ci, H. You, L. Yan, K. Chen, N. Zhao, C. Xu, J. Lan, D. Liu, J. Zhang, Z. Shi, Q. Wu, K. Yang, L. Zhao, Z. Qiu, D. Lv, W. Gao, H. Yang, F. Lin, Q. Wang, J. Man, C. Li, W. Tao, S. Agnihotri, X. Qian, S.C. Mack, N. Zhang, Y. You, J.N. Rich, G. Sun, X. Wang, Dual role of CXCL8 in maintaining the mesenchymal state of glioblastoma stem cells and M2-like tumor-associated macrophages, Clin. Cancer Res. 29 (2023) 3779–3792, https://doi.org/10.1158/1078-0432.CCR-22-3273.
[37] F. Khan, L. Pang, M. Dunterman, M.S. Lesniak, A.B. Heimberger, P. Chen, Macrophages and microglia in glioblastoma: heterogeneity, plasticity, and therapy, J. Clin. Invest. 133 (2023) e163446, https://doi.org/10.1172/JCI163446.
[38] M.A. Heinrich, R. Bansal, T. Lammers, Y.S. Zhang, R. Michel Schiffelers, J. Prakash, 3D-bioprinted Mini-brain: a glioblastoma model to study cellular interactions and therapeutics, Adv. Mater. 31 (2019) e1806590, https://doi.org/10.1002/adma.201806590.
[39] F.U. Rehman, Y. Liu, Q. Yang, H. Yang, R. Liu, D. Zhang, P. Muhammad, Y. Liu, S. Hanif, M. Ismail, M. Zheng, B. Shi, Heme Oxygenase-1 targeting exosomes for temozolomide resistant glioblastoma synergistic therapy, J. Control. Release 345 (2022) 696–708, https://doi.org/10.1016/j.jconrel.2022.03.036.
[40] T.A. Mishchenko, V.D. Turubanova, E.N. Gorshkova, O. Krysko, M.V. Vedunova, D. V. Krysko, Targeting immunogenic cell death for glioma immunotherapy, trends, Cancer 10 (2024) 8–11, https://doi.org/10.1016/j.trecan.2023.10.005.
[41] T. Wang, M. Han, Y. Han, Z. Jiang, Q. Zheng, H. Zhang, Z. Li, Antigen self-presented personalized nanovaccines boost the immunotherapy of highly invasive and metastatic tumors, ACS Nano 18 (2024) 6333–6347, https://doi.org/10.1021/acsnano.3c11189.
[42] A. Sabbagh, K. Beccaria, X. Ling, A. Marisetty, M. Ott, H. Caruso, E. Barton, L. Y. Kong, D. Fang, K. Latha, D.Y. Zhang, J. Wei, J. DeGroot, M.A. Curran, G. Rao, J. Hu, C. Desseaux, G. Bouchoux, M. Canney, A. Carpentier, A.B. Heimberger, Opening of the blood-brain barrier using low-intensity pulsed ultrasound enhances responses to immunotherapy in preclinical glioma models, Clin. Cancer Res. 27 (2021) 4325–4337, https://doi.org/10.1158/1078-0432.CCR-20-3760.
[43] M. Swiecki, M. Colonna, The multifaceted biology of plasmacytoid dendritic cells, Nat. Rev. Immunol. 15 (2015) 471–485, https://doi.org/10.1038/nri3865.
[44] M. Kilian, R. Sheinin, C.L. Tan, M. Friedrich, C. Krämer, A. Kaminitz, K. Sanghvi, K. Lindner, Y.-C. Chih, F. Cichon, B. Richter, S. Jung, K. Jähne, M. Ratliff, R. M. Prins, N. Etminan, A. von Deimling, W. Wick, A. Madi, L. Bunse, M. Platten, MHC class II-restricted antigen presentation is required to prevent dysfunction of cytotoxic T cells by blood-borne myeloids in brain tumors, Cancer Cell 41 (2023) 235–251.e9, https://doi.org/10.1016/j.ccell.2022.12.007.
[45] H. Liu, W. Qiu, T. Sun, L. Wang, C. Du, Y. Hu, W. Liu, F. Feng, Y. Chen, H. Sun, Therapeutic strategies of glioblastoma (GBM): the current advances in the molecular targets and bioactive small molecule compounds, Acta Pharm. Sin. B 12 (2022) 1781–1804, https://doi.org/10.1016/j.apsb.2021.12.019.
[46] Q. Xu, K. Huang, X. Meng, Y. Weng, L. Zhang, L. Bu, X. Zheng, J. Cai, R. Zhan, Q. Chen, Safety and efficacy of anlotinib hydrochloride plus temozolomide in patients with recurrent glioblastoma, Clin. Cancer Res. 29 (2023) 3859–3866, https://doi.org/10.1158/1078-0432.CCR-23-0388.